BHM (2010) Vol. 155(11): 499 – 505
DOI 10.1007/ s00501-010-0614-3
Printed in Austria

BHM Berg- und Hüttenmännische Monatshefte

TEM Investigation of a Novel Fe Containing Phase in High Purity Al-Si-Fe Alloys

Jiehua Li*, Muhammad Zarif* and Peter Schumacher*, **

* Chair of Casting Research, University of Leoben, Leoben, Austria
** Austrian Foundry Research Institute, Leoben, Austria

Received: September 27, 2010; accepted: October 5, 2010

Abstract: A novel Fe containing phase has been investigated by Transmission Electron Microscopy (TEM) and designated as F_1 (FCC, a = 1.60 nm) in a series of high purity Al-5Si alloys (wt %) with a 200 ppm Fe addition after rapid quenching. During heating up to 600 °C in DSC, more Fe containing phases precipitate and have been designated as F_2 for comparison. The size of the plate-shaped F_2 phase is more than 500 nm in length and about 5 nm in width, with a ratio of about 100:1. It is much larger than that of the F_1 phase, suggesting the F_1 phase grows and coarsens during heating, while the crystal structure of F_2 phase remains unchanged, indicating the F_1 phase has a high thermal stability and no phase transformation occurs up to 600 °C. The addition of Sr and/or P decreases the solubility of Fe in α-Al matrix, which leads to more Fe containing phase precipitate after rapid quenching. The effect of impurity on the phase selection in Al-5Si alloys is also discussed.

TEM-Untersuchung der neuen Fe-haltigen Phase in hochreinen Al-Si-Fe-Legierungen

Zusammenfassung: Eine neue ausgeschiedene Fe-haltige Phase in hochreinen Al-5Si- Legierungen (mit 200 ppm Fe) wurde nach schneller Abkühlung mittels TEM untersucht und als F_1 (FCC, a = 1,60 nm) bezeichnet. Es wurde festgestellt, dass während des Aufheizens im DSC-Tiegel bis 600 °C mehrere Fe-haltige Phasen als F_2 im Vergleich mit anderen ausgeschieden werden können. Die blechgeformte F_2 weist Längen größer als 500 nm und Breiten von ca. 5 nm im Verhältnis 100:1 auf. Die F_2 ist größer als die F_1, wobei die F_1 während des Aufheizens gewachsen ist bzw. vergröbert wurde, die Kristallographiestruktur der F_2-Phase jedoch konstant blieb. Weiters wurde festgestellt, dass die F_1-Phase hoch temperaturbeständig ist und keine neue Phase bzw. Phasenumwandlung bei 600 °C auftreten kann. Mit Zugaben von Sr und/oder P wird die Löslichkeit des Fe in der Al-5Si-Legierung bzw. Matrix vermindert, was zu mehreren Ausscheidungen der Fe-haltigen Phase nach schneller Abkühlung oder Abschreckung führt. In weiterer Folge wurde der Einfluss der Spurenelemente auf die Phasenumwandlung in der Al-5Si-Legierung diskutiert.

1. Introduction

Iron is a natural impurity in aluminium and aluminium alloys arising during the production of primary aluminium via the Bayer process that converts bauxite (the ore) into alumina (the feedstock) and the Hall-Héroult electrolytic reduction process converting alumina into molten aluminium (900 °C) with the consumption of both electricity and carbon. The further melting and casting activities can also increase the iron level via the reaction with unprotected steel tools and the addition of low-purity alloying materials, e. g. Si[1]. It is usually considered that iron has detrimental effects on the ductility and castability in casting/foundry alloys, particularly for Al-Si based alloys, although iron can also be a deliberate alloying addition to improve the processing capabilities of the alloy and/or the strength of final products in certain wrought aluminium alloys[2]. These detrimental effects can be attributed to the formation of a variety of stable and metastable intermetallic phases, depending upon alloy composition and solidification rate[3–5].

The Fe containing intermetallic phases in 1XXX Al alloys[6], 3XXX Al alloys[7, 8], 6082 Al alloys[9–11], have been widely investigated after conventional casting, i.e. direct chill casting, gravity casting, etc. It is generally accepted that the Al_8Fe_2Si (known as alpha- or α-phase) and Al_5FeSi (known as beta- or β-phase) are the dominant phases in Al-Si-Fe alloys. Some other Fe containing phases, i.e. $Al_8FeMg_3Si_6$ (known as π-phase) and $Al_{15}(Fe,Mn)_3Si_2$ (known as α-phase), can also form when Si is added with Mg, Mn etc. However, the Fe containing intermetallic phases after conventional casting often consist of large plates of inter-

Correspondence author:
Dr. Jiehua Li
Lehrstuhl für Gießereikunde, Montanuniversität Leoben,
Franz-Josef Straße 18, 8700 Leoben, Austria
e-mail: jiehua.li@unileoben.ac.at

metallics along the grain boundary that give rise to inferior mechanical properties. For example, the morphology of the β-phase is plate-like with a thickness of a few tenths of a micrometre and other dimensions of the order of 10 μm, although α-phase is a less Si-rich and more spheroidised phase than β-phase. Very little success has been achieved either by heat treatment or by the addition of modifiers and refiners during the conventional casting process. The benefit of rapid solidification techniques like melt spinning and spray casting etc. has been well understood in synthesising aluminium alloys for high-temperature application[5, 6].

Indeed, the Fe containing intermetallic phases in Al-Si-Fe alloys after rapid solidification, i.e. gas atomisation[12, 13], melt spinning[14–20], spray casting[21–23], etc. have also been investigated. It has been reported that the formation of β-phase can be suppressed and refined by increasing the cooling rates to those typical for rapid solidification processes (10^6 K/s), and a wider variety of Fe containing phases can form after rapid solidification[23]. A δ-Al4Si2Fe phase (tetragonal structure, with lattice parameters a = 1.26–1.3 nm; c = 0.37 nm) was reported to form in atomised powder particles in an Al-18Si-5Fe-1.5Cu (wt. %) alloy[22, 23]. During a slow cooling of the spray deposit, the δ-Al4Si2Fe phase was transformed to a cellular and plate-like morphology of β-Al_5FeSi phase. More interestingly, some novel Fe containing phases, i.e. q_1-AlFeSi, precipitated under conditions of fairly fast solidification (10 K/s) in a dilute Al-0.25Fe-0.13Si (wt %) alloy, and this phase transformed to another novel phase denoted as q_2-AlFeSi upon heat treatment for 14 h at 873 K[24, 25]. The crystal symmetry of q_1-AlFeSi (Cmmm, C-centred orthorhombic structure, with lattice parameters a = 1.27, b = 3.62, c = 1.27 nm), q_2-AlFeSi (Pm, monoclinic structure with lattice parameters a = 1.25, b = 1.23, c = 1.93 nm, β = 109°), and the crystallographic orientation relationships between these two Al-Fe-Si phases and α-Al has been also determined by electron diffraction and convergent beam electron diffraction[24–26]. However, the morphologies of q_1-AlFeSi and q_2-AlFeSi phases are still similar to that after conventional casting owing to the relatively slow cooling rates, although the sizes are refined to about 1–3 μm. No previous research reports are devoted to the nanoscale Fe containing phase in Al-Si-Fe alloy produced by a higher cooling rate. More importantly, the alloys mentioned above are almost prepared by using commercial purity aluminium. Apart from Fe and Si, it is unavoidable to contain some small quantities of impurities, i.e. Ti, Ni, Cr, Sr, P etc. These impurities are believed to play an important role in heterogeneous nucleation during solidification and control the formation and microstructure of equilibrium and metastable phases, especially for Sr and P in Al-Si alloys[27]. The research on a high purity Al-Si-Fe alloy is of great interest to elucidate the impurity effect on the formation of Fe containing phase.

Here, we report some preliminary TEM investigations on a novel nanoscale Fe containing phase in a series of high purity Al-5Si-Fe (only 200 ppm) alloys with trace elements of Sr and P addition produced by melt spinning. The primary aim of this paper is not only to characterise the novel Fe containing phase, but also to reveal the effects of trace Sr, P impurities on nucleation and phase selection in Al-Si-Fe alloys. The microstructure evolution depending on the thermal history of the melt-spinning Al-5Si-Fe alloys is also highlighted in this paper.

2. Experiments

A series of high purity Al-5Si-Fe alloys (wt %) with a trace addition of Sr and P elements were prepared by using arc melting and melt spinning. It should be noted that an Al-19Cu-1.4P (wt %) rod, manufactured by Technologica GmbH, was used for the addition of P in the Al-Si-Sr-P alloy. This Al-Cu-P rod is not based on a high purity Al material. Thus, some impurities, such as Fe, Cu, were also added into the Al-Si-Sr-P alloy. All the other elements (Al, Si and Sr) were added from high purities materials. Al was added with a 4N super purity electrolytically refined Al produced by Hydro Aluminium High Purity GmbH. Si was added with a 5N and 4N purity Si produced by Siltronic AG and SAG GmbH. Sr was added with a Al-3.59 wt % Sr master alloy manufactured by a 4N Al and 99 wt % Sr (Johnson Matthey PLC). The composition was analysed by OES spark analysis and the result is given in Table 1. For simplicity, the alloys are short for Alloy A, Alloy B and Alloy C, respectively.

TABLE 1:
Chemical composition of the Al-Si-Fe alloys with a trace addition of Sr and P obtained from OES spark analysis (wt. %)

Alloy No.	Al	Si	Fe	Sr	P
Alloy A	Balance	5.00	0.02	–	–
Alloy B	Balance	5.00	0.005	0.01	–
Alloy C	Balance	5.00	<0.005	0.02	0.003

The ingots were arc melted at least three times on a water cooled Cu hearth in a 200 mbar Ar atmosphere. The ingots were sectioned to about 2–3 g portions, remelted in a quartz crucible by close-loop controlled radio frequency heating with a two colour pyrometer, and then melt-spun on a Cu wheel with a rotating speed of 15 ms^{-1} under a reduced (200 mbar) He (99.998 %) atmosphere with a super heat (ΔT) about 125 °C, a pressure difference (ΔP) about 100 mbar. Typical ribbons were about 2–3 mm in width and 70–80 μm in thickness.

The as-quenched ribbons of about 5 mg weight were heated and then cooled in the range from 600 °C to 400 °C with a rate of 10 °C/min in a power compensated DSC (Perkin-Elmer Diamond), with an aim to investigate the microstructure evolution depending on the thermal history. The ribbons before (as-quenched) and after heating in DSC were mechanically ground, polished and dimpled to about 30 μm, and then ion-beam milled with a low angle of 4° and a low voltage of 4 kV using a Gatan Precision Ion Polishing System (PIPS, Gatan model 691). Transmission electron microscopy (TEM) was performed using a Philips CM12 microscopy operated at 120 kV and a JEOL-2100F with a Cs-corrected microscopy operated at 200 kV. The EDX analysis was performed in CM12.

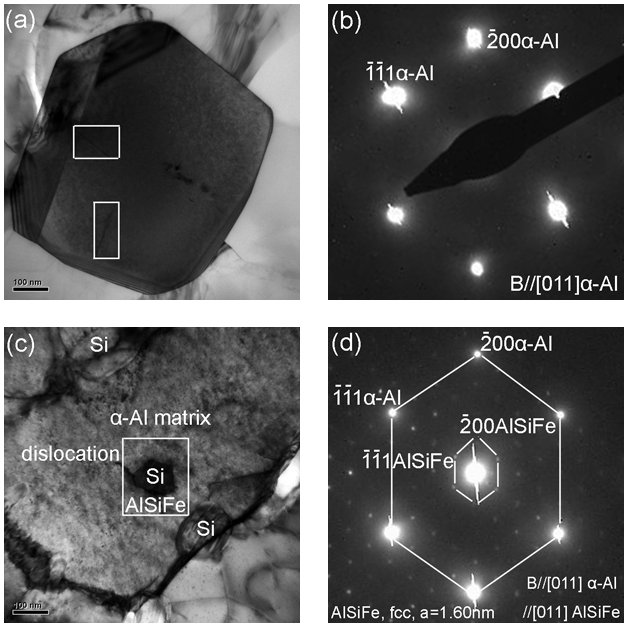

Fig. 1: TEM bright field micrographs (a), (c) and selected area diffraction pattern (b), (d) taken from Al-5Si-200 ppm Fe (wt. %) alloys after rapid quenching. Incident electron beam direction is parallel to $[011]_{\alpha\text{-Al}}$. Diffraction spots are indexed by a cubic Al-crystal

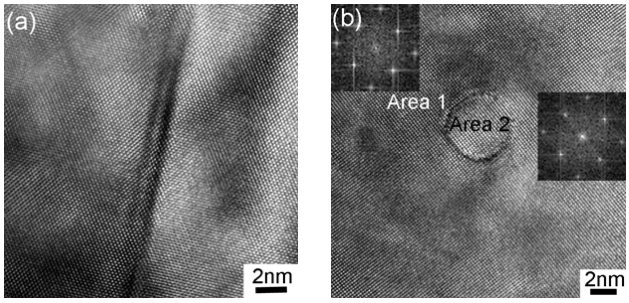

Fig. 2: High-resolution TEM image of the needle Fe containing phase (a), the small Si crystal precipitated from α-Al matrix (b), taken from Al-5Si-200 ppm Fe (wt %) alloy after rapid quenching. Incident electron beam direction is parallel to $[011]_{\alpha\text{-Al}}$. The FFT was inserted in the figures

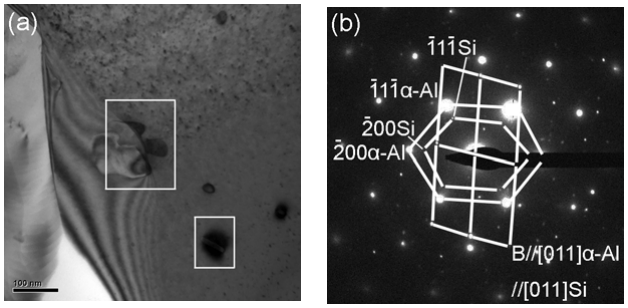

Fig. 3: TEM bright field micrographs (a) and selected area diffraction pattern (b) of Fe containing phase and the connected Si crystals taken from Al-5Si-200 ppm Fe (wt. %) alloys after rapid quenching. Incident electron beam direction is parallel to $[011]_{\alpha\text{-Al}}$. Diffraction spots are indexed by a cubic Al-crystal

3. Results and Discussion

3.1 Fe Containing Phases in Al-5Si-Fe Alloy after Rapid Quenching

Figure 1 shows the TEM bright field micrographs (a), (c) and corresponding selected area diffraction pattern (SADP) (b), (d), taken from Al-5Si-200 ppm Fe (wt. %) alloys after rapid quenching. No clear Fe containing phases are present in the microstructure, as shown in Fig. 1a, and no clear diffraction streaks from Fe containing phases are evident in the $[011]_{\alpha\text{-Al}}$ SADP, as shown in Fig. 1b, suggesting that Si and Fe are mainly dissolved into α-Al matrix owing to the higher cooling rate during melt spinning. This is consistent with the report in an as-quenched Al-7.6Si-3.3Fe alloy[20], where only the α-Al solid solution peaks and a small Si peak are present in XRD patterns. It should be noted that the Fe content in this study is much lower than that in Al-7.6Si-3.3Fe alloy. Thus, it seems to make sense that there is no Fe containing phase formed during melt spinning. However, more careful observation reveals that some needles are present in the microstructure, as marked with white box in Fig. 1a. These needles are about 100 nm in length and about 1 nm in width, as shown in Fig. 2a. Some Si particles spherical in shape ranging from 5 to 50 nm in size are also present in the microstructure, as marked with white box in Fig. 1c and shown in Fig. 2b. The Si particle in Fig. 1c seems to be connected with some Fe containing phase (at the edge of the Si particle) and a random dislocation. Thus, we suppose that the Si particle and Fe containing phase come from the impurities during the alloy preparation and/or the uncompleted melting activities. During melt spinning, these impurities survive in the ribbons, and nucleate the α-Al phase. The corresponding SADP, as shown in Fig. 1d, indicates that these Fe containing phases possess a face-centred cubic unit cell with a = 1.60 nm. The crystallographic orientation relationships between these Al-Fe-Si phases and α-Al matrix keep a perfect cubic to cubic relationship, i.e. (200)AlSiFe<011>AlSiFe//(200) α-Al <011> α-Al. It should be noted that these Fe containing phases are different from the previous reports, although some Fe containing phase with a face-centred cubic unit cell with a = 1.23 nm has also been reported[6]. Given the unique solidification condition, and the addition high purity Al, Si and only a 200 ppm Fe, it is reasonable to expect some novel Fe containing phases may occur. For compassion and simplification, these novel Fe containing phases are designated as F_1 (FCC, a = 1.60 nm) here.

Figure 3 shows other TEM bright field micrographs (a) and corresponding SADP (b) taken from the same sample. As marked with white box in Fig. 3a, some Si particles are also connected with some Fe containing phase. The corresponding SADP (Fig.3b) indicates that these Si particles and α-Al matrix also keep a perfect cubic to cubic relationship, although the Fe containing phase can not be indexed correctly owing to unclear diffraction streaks. This orientation relationship can also be confirmed by the fast Fourier transform (FFT) image as inserted in Fig. 2b. The left FFT is from α-Al matrix (Area 1), and the right FFT is from small Si particle (Area 2). They keep a perfect cubic to cubic relationship.

Apart from the small Si particles in the α-Al matrix, some large Si crystals are also present along the grain boundary. As shown in Fig. 4a, the Si crystal is about 200 nm in size. Some unclear twins appear on the Si crystal, suggesting

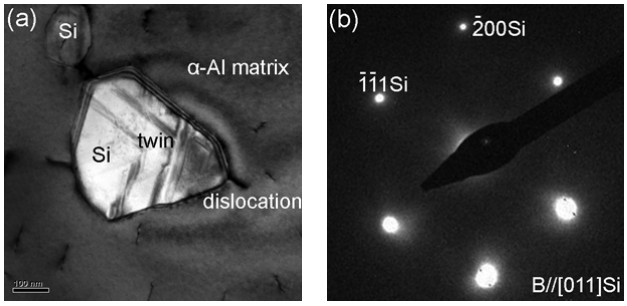

Fig. 4: TEM bright field micrographs (a) and selected area diffraction pattern (b) of the twin in Si crystals taken from Al-5Si-200 ppm Fe (wt. %) alloys after rapid quenching. Incident electron beam direction is parallel to [011] $_{\alpha\text{-Al}}$

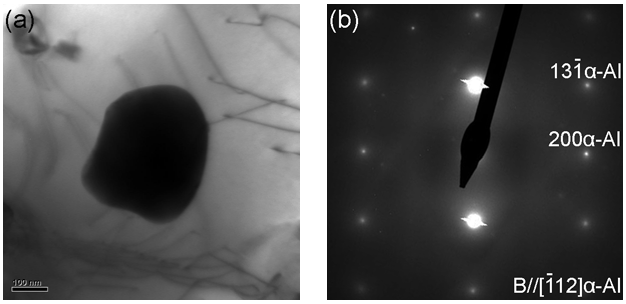

Fig. 5: TEM bright field micrographs (a) and selected area diffraction pattern (b) of some impurity particles taken from Al-5Si-200 ppm Fe (wt. %) alloys after rapid quenching. Incident electron beam direction is parallel to [-112] $_{\alpha\text{-Al}}$. Diffraction spots are indexed by a cubic Al-crystal

the mechanism of impurity-induced-twin Si crystal may be applicable. Similar to Fig. 1c, some dislocations are also present in the microstructure. These dislocations may be attributed to the residual strain induced during the rapid quenching or the TEM sample preparation. However, no clear diffraction streaks from Fe containing phases are evident in the corresponding [011] $_{\alpha\text{-Al}}$ SADP, as shown in Fig. 4b, suggesting that these Si crystals are not nucleated at the edge of the Fe containing phase.

Figure 5 shows TEM bright field micrographs (a) and selected area diffraction pattern (b) of some impurity particles taken from the same sample. As described in part 2, the alloys studied here are prepared with a high purity Al and Si addition. However, some impurity particles are still present in the microstructure. After some tilting experiment, these impurity particles are found to be round with a diameter of about 200 nm. EDX results (not shown here) confirmed that theses impurity particles are rich in Ti, Cu, Cr etc. However, the crystallographic orientation relationships between these impurity particles and α-Al matrix fail to obtain from the corresponding SADP, as shown in Fig. 5b, because these particles are too thick to obtain a clear diffraction streak. As shown Fig. 5a, these impurity particles are only connected with some dislocation. Thus, it can be expected that these impurity particles are not involved into the nucleation and phase selection during melt spinning. However, as described in the next part, the impurity particles indeed nucleated the Fe containing phase during heating up to 600 °C.

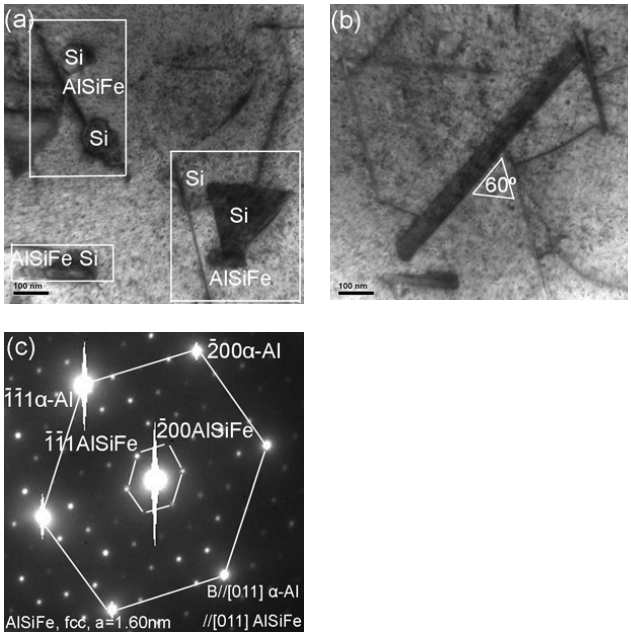

Fig. 6: TEM bright field micrographs (a), (b), selected area diffraction pattern (c) of Fe containing phase, taken from Al-5Si-200 ppm Fe (wt. %) alloys after heating up to 600 °C in DSC. Incident electron beam direction is parallel to [011] $_{\alpha\text{-Al}}$. Diffraction spots are indexed by a cubic Al-crystal

3.2 Fe Containing Phase in Al-5Si-Fe Alloy after Heating up to 600 °C

Figure 6 shows the TEM bright field micrographs (a), (b), selected area diffraction pattern (c) of the Fe containing phase, taken from Al-5Si-200ppm Fe (wt. %) alloys after heating up to 600 °C in DSC. After heating, increased nucleation of Fe containing phases are observed. For comparison to F_1, these Fe containing phases are designated as F_2 here. The morphology of the F_2 phases seems to be plate-like. The size of the plate-shaped F_2 phase is more than 500 nm in length and about 5 nm in width, with a ratio of about 100:1, as shown in Fig. 6b. It is much larger than that of the F_1 phase, suggesting the F_1 phase grows and coarsens during heating, while the crystal structure of F_2 phase remains unchanged, although the intensity of the diffraction streak becomes stronger, as shown in Fig. 6c, indicating that the F_1 phase has a high thermal stability and no phase transformation occurs up to 600 °C. More interestingly, the plate-shaped Fe containing phases are almost connected with Si crystal, as marked with white box in Fig. 6a. It is very clear that the Si crystals are nucleated to the Fe containing phases during the heating process. It should be also noted that the angles between these Fe containing phases are about 60°, and the Fe containing phases are distributed along three directions, as marked in Fig. 6b. This is different from the result of the Al-Si-Fe-Sr/P alloy with a trace Sr and P addition, as described in the next part.

As expected, the Si crystal along the grain boundary also grows and coarsens during heating, as shown in Fig. 7. The size of these Si crystals is about 5–10 μm after heating. Only small parts of the twins survive after heating, as shown in Fig. 7a. Some small Si particles precipitate along the twins, as shown in Fig. 7b. In contrast to Fig. 6a, no Fe

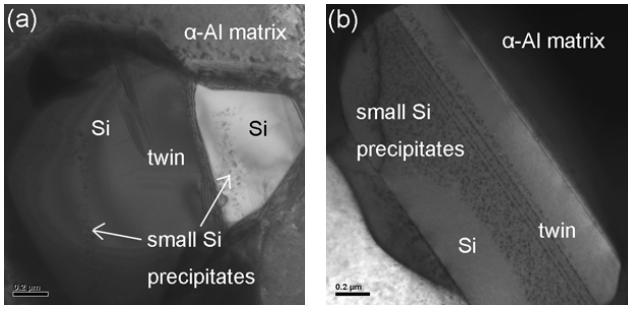

Fig. 7: TEM bright field micrographs of the disappeared twin (a) and some small scale Si precipitates along the twin (b) in the Si crystals taken from Al-5Si-200 ppm Fe (wt. %) alloys after heating up to 600 °C in DSC. Incident electron beam direction is parallel to [011] $_{\alpha\text{-Al}}$

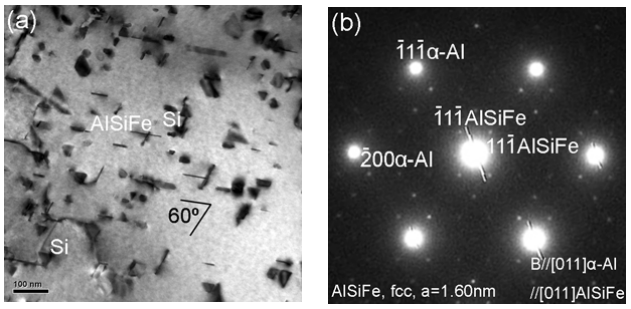

Fig. 9: TEM bright field micrographs (a) and selected area diffraction pattern (b) taken from Al-5Si-100ppm Sr-50 ppm Fe (wt. %) alloys after rapid quenching. Incident electron beam direction is parallel to [011] $_{\alpha\text{-Al}}$

containing phase is connected with these Si crystals along the grain boundary, suggesting again that the Si crystals along the grain boundary are not nucleated at the edge of the Fe containing phases.

As mentioned above, the impurity particles are found to be involved in the formation of the Fe containing phases during heating. Figure 8 shows the TEM bright field micrographs (a), selected area diffraction pattern (b), and EDX results of the α-Al matrix (c) and the impurity particle (d), taken from the same sample. For EDX analysis, it should be noted that the sample has been tilted not to be at a zone axis, and the peak of Cu can be attributed to the Cu ring where the TEM samples are mounted. It is very clear that there is no strong peak coming from the impurity in the α-Al matrix, while the impurity particles are rich in Ti, V, Cr and Sr, P etc., as shown in Fig. 8d. As mentioned above, some impurity particles are present in the microstructure after melt spinning. It is reasonable to expect that these impurity particles still exist during heating. Moreover, as marked with white arrow in Fig. 8a, the impurity particles are connected to Fe containing phases, suggesting Fe containing phase may be nucleated on impurity particles.

3.3 Fe Containing Phase in Al-5Si-Fe-Sr/P Alloy after Rapid Quenching

Figure 9 shows the TEM bright field micrographs (Fig.9a) and SADP (Fig.9b) taken from Al-5Si-100 ppm Sr-50 ppm Fe (wt. %) alloys after rapid quenching. In contrast to the Al-Si-Fe alloy without Sr addition, the Fe containing phases are present in the microstructure, although the Fe content is only 50 ppm, much lower than that (200 ppm) in Al-Si-Fe alloy, suggesting the addition of Sr promotes the formation of the Fe containing phases in Al-Si-Fe alloy. This may be attributed to the decrease of the Fe solubility in α-Al matrix. The same is also true to the Al-Si-Sr-P alloy. As shown in Fig. 10, the Fe containing phases are in a high quantity in the microstructure, although the Fe content is less than 5 ppm, much lower than that (200 ppm) in Al-Si-Fe alloy. It

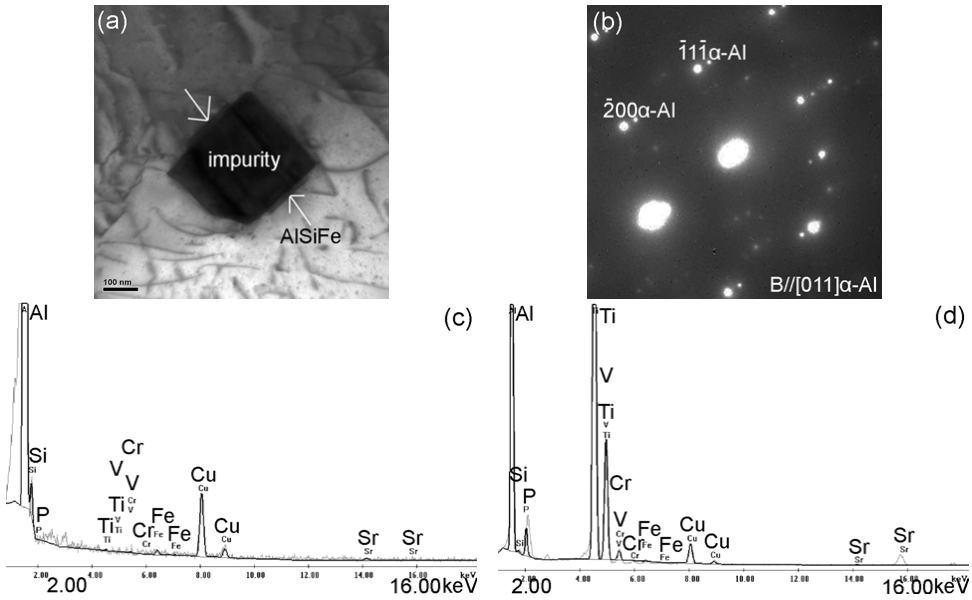

Fig. 8: TEM bright field micrographs (a), selected area diffraction pattern (b), and EDX results of the α-Al matrix (c) and the impurity particle connected to Fe containing phase (d), taken from Al-5Si-200 ppm Fe (wt. %) alloys after heating up to 600 °C in DSC. Incident electron beam direction is parallel to [011] $_{\alpha\text{-Al}}$. For EDX analysis, the samples were tilted not to be at a zone axis

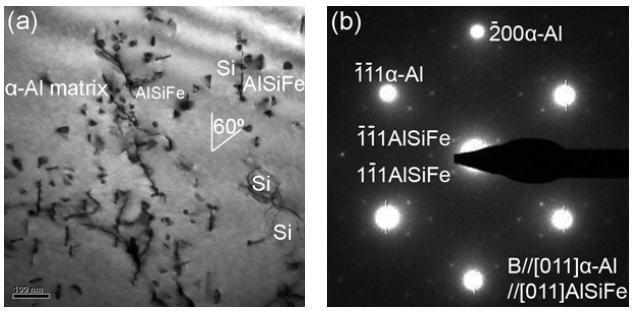

Fig. 10: TEM bright field micrographs (a) and selected area diffraction pattern (b) taken from Al-5Si-200ppm Sr-5ppm P (wt. %) alloy after rapid quenching. Incident electron beam direction is parallel to $[011]_{\alpha\text{-Al}}$

is very clear that the impurity of Sr and P has a great effect on the formation of Fe containing phase. It should be noted that these Fe containing phases are nanoscale in size, plate-like in morphology, and distributed in only two directions, as marked in Fig. 9a and Fig. 10a. This is different from the Al-Si-Fe alloy after heating, where the Fe containing phases are distributed along three directions. It is not surprising that the diffraction streak from Al-Si-Sr-Fe alloy and Al-Si-Sr-P alloy is present in only two directions in the corresponding SADP, as shown in Fig. 9b and Fig. 10b, respectively. The diffraction streak along (200) reflection is not evident in both SADPs. It should be also noted that these Fe containing phases are almost connected with some small Si particles in the α-Al matrix, suggesting that these nanoscale Si particles may be nucleated to these Fe containing phases. It is also interesting that some nanoscale Si particles seem to be triangular-like. These triangular shaped Si particles have not been reported in the previous research. It can be seen more clearly in Fig. 11 when the same sample is tilted to <111> zone axis. The TEM bright field and dark field images (using the diffraction streak from the Fe containing phase) clearly show that the triangular shaped Si particles are present in the microstructure. This is also consistent with Fig. 6a, where a triangular shaped Si particle is connected with a Fe containing phase although the size is larger after heating. The corresponding <111> SADP (Fig. 11c) also shows that the crystallographic orientation relationships between these Al-Fe-Si phases, Si particles and α-Al matrix keep a perfect orientation relationship, i.e. (200) AlSiFe<111>AlSiFe //(200)Si<111>Si //(200) α-Al <111> α-Al, indicating again that the Fe containing phases have a high potency to nucleate the Si and α-Al phase. Similar to the Al-Si-Fe alloy, all the SADPs (Fig. 9b, Fig. 10b and Fig. 11c) from Al-Si-Sr-Fe alloy and Al-Si-Sr-P alloy can also be indexed to be a fcc unit cell with a lattice parameter a = 1.60 nm, suggesting that the addition of Sr and P only promotes the formation of the Fe containing phase, but does not change the structure. Further investigations on the transformation process of these novel Fe containing phases are under progress. The results are beyond the scope of this paper, and will be reported elsewhere.

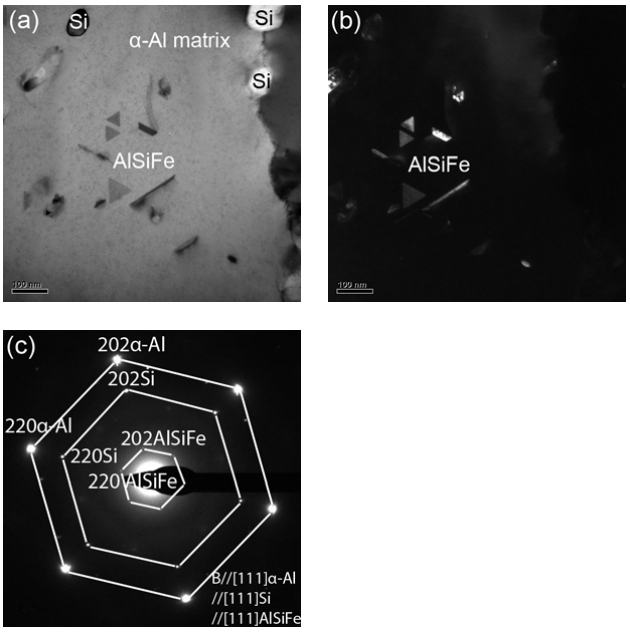

Fig. 11: TEM bright field micrographs (a), dark field micrographs (b) and selected area diffraction pattern (c) taken from Al-5Si-200 ppm Sr-5 ppm P (wt. %) alloy after rapid quenching. Incident electron beam direction is parallel to $[111]_{\alpha\text{-Al}}$

4. Conclusions

The Fe containing phases are very complex in Al alloy, especially for the high purity Al-Si-Fe alloy. Here, we report a novel Fe containing phase in a series of high purity Al-5Si alloys (wt %) with a 200 ppm Fe addition. These Fe containing phases are nanoscale in size, plate-like in morphology, and have a good thermal stability during heating up to 600 °C. The impurities of Sr and P are also found to have a great influence on the formation of the Fe containing phases. The present TEM investigation can provide some complementary information to understand the nucleation and phase selection in Al-Si-Fe alloys.

Acknowledgements

Jiehua Li gratefully acknowledges Mrs Gabriele Moser, Dr. Rashkova Boriana for their kind help on TEM sample preparation, and Dr. Thomas Jörg and Dr. Zaoli Zhang for their help on JEOL – 2100F TEM in Erich Schmid Institute of Materials Science.

References

1 *Taylor, J.A.*: The effect of iron in Al-Si casting alloys. In: *J. Couzner* et al., Casting Concepts. 35th Australian Foundry Institute National Conference, Adelaide, South Australia (2004).

2 *Dash, M., and M. Makhlouf*: Effect of key alloying elements on the feeding characteristics of aluminium-silicon casting alloys. Journal of Light Metals, 1 (2001), 251–265.

3 *Moustafa, M.A.*: Effect of iron content on the formation of β-Al_5FeSi and porosity in Al-Si eutectic alloys. Journal of Materials Processing Technology, 209 (2009), 605–610.

4 *Seifeddine, S., S. Johansson, and I.L. Svensson*: The influence of cooling rate and manganese content on the β-Al_5FeSi phase formation and mechanical properties of Al-Si-based alloys. Materials Science and Engineering A, 490 (2008), 385–390.

5 *Dutta, B., and M. Rettenmayr*: Effect of cooling rate on the solidification behaviour of Al-Fe-Si alloys. Materials Science and Engineering A, 283 (2000), 218–224.

6 *Allen, C.M., K.A.Q. O'Reilly, B. Cantor, and P.V. Evans*: Intermetallic phase selection in 1XXX Al alloys. Progress in Materials Science, 43 (1998), 89–170.

7 *Ashtari, P., H. Tezuka, and T. Sato*: Modification of Fe-containing intermetallic compounds by K addition to Fe-rich AA319 aluminium alloys. Scripta Materialia, 53 (2005), 937–942.

8 *Alexander, D.T.L., and A.L. Greer*: Solid-state intermetallic phase tranformations in 3XXX aluminium alloys. Acta Materialia, 50 (2002), 2571–2583.

9 *Mrówka-Nowotnik, G., J. Sieniawski, and M. Wierzbińska*: Intermetallic phase particles in 6082 aluminium alloy. Archives of Materials Science and Engineering, 2(28) (2007), 69–76.

10 *Kuijpers, N.C.W., W.H. Kool, P.T.G. Koenis, K.E. Nilsen, I. Todd, and S.van der. Zwaag*: Assessment of different techniques for quantification of α-Al(FeMn)Si and β-AlFeSi intermetallics in AA 6XXX alloys. Materials Characterization, 49 (2003), 409–420.

11 *Sha, G., K.A.Q. O'Reilly, B. Cantor, J. Worth, and R. Hamerton*: Growth related metastable phase selection in a 6XXX series wrought Al alloy. Materials Science and Engineering A, 304–306 (2001), 612–616.

12 *Zhang, L.C., A.Q. He, H.Q. Ye, C. Huang, and Y.C. Zhang*: Characterization of dispersed intermetallic phases in an Al-8.32 wt%Fe-3.4 Wt%Ce alloy. Journal of Materials Science, 37 (2002), 5183–5189.

13 *Park, W.W., B.S. You, and N.J. Kim*: Microstructure and mechanical properties of rapidly solidified Al-Si-Fe-X base alloys. Materials and Design, 5–6(17) (1996), 255–259.

14 *Allen, C.M., K.A.Q. O'Reilly, P.V. Evans, and B. Cantor*: The effect of vanadium and grain refiner additions on the nucleation of secondary phases in 1XXX Al alloys. Acta Mater, 17(47) (1999), 4387–4403.

15 *Allen, C.M., K.A.Q. O'Reilly, and B. Cantor*: Effect of semisolid microstructure on solidified phase content in 1XXX Al alloys. Acta Mater, 49 (2001), 1549–15633.

16 *Allen, C.M., K.A.Q. O'Reilly, B. Cantor, and P.V. Evans*: Heterogeneous nucleation of solidification of equilibrium and metastable phases in melt-spun Al-Fe-Si alloys. Materials Science and Engineering A, 226–228 (1997), 784–788.

17 *Schumacher, P., and P. Cizek*: Heterogeneous nucleation mechanism in Al-Fe-Si amorphous alloys. Materials Science and Engineering A, 304–306 (2001), 215–219.

18 *Rajabi, M., M. Vahidi, A. Simchi, and P. Davami*: Effect of rapid solidification on the microstructure and mechanical properties of hot-pressed Al-20Si-5Fe alloys. Materials Characterization, 60 (2009), 1370–1381.

19 *Ünlü, N., A. Genç, M.L. Öveçoğlu, N. Eruslu, and F.H. Froes*: Characterization investigation of melt-spun ternary Al-χSi-3.3Fe (χ=10, 20 wt.%) alloys. Journal of Alloys and Compounds, 322 (2001), 249–256.

20 *Ünlü, N., A. Genç, M.L. Öveçoğlu, E.J. Lavernia, and F.H. Froes*: Microstructural evolution during annealing of the melt-spun ternary hypoeutectic Al-7.6Si-3.3Fe (in wt.%) alloy. Journal of Alloys and Compounds, 343 (2002), 223–233.

21 *L.G. Hou, C. Cui, and J.S. Zhang*: Optimizing microstructures of hypereutectic Al-Si alloys with high Fe content via spay forming technique. Materials Science and Engineering A, 527 (2010), 6400–6412.

22 *Srivastava, V.C., P. Ghosal, and S.N. Ojha*: Microstructure and phase formation in spay-deposited Al-18 %Si-5 %Fe-1.5 %Cu alloy. Materials Letters, 56 (2002), 797–801.

23 *Srivastava, A.K., V.C. Srivastava, A. Gloter, and S.N. Ojha*: Microstructural features induced by spray processing and hot extrusion of Al-18 %Si-5 %Fe-1.5 %Cu alloy. Acta Materialia, 54 (2006), 1741–1748.

24 *Liu, P., and G.L. Dunlop*: Determination of the crystal symmetry of two Al-Fe-Si phases by convergent-beam electron diffraction. J. Appl. Cryst, 20 (1987), 425–427.

25 *Liu, P.,* and *G.L. Dunlop*: Symmetry determination by CBED of two recently discovered Al-Fe-Si phases. Ultramicroscopy, 4(19) (1986), 405.

26 *Liu, P., and G.L. Dunlop*: Crystallographic orientation relationships for Al-Fe and Al-Fe-Si precipitates in Aluminium. Acta Metallurgica, 6(36) (1988), 1481–1489.

27 *Cantor, B.*: Impurity effects on heterogeneous nucleation. Materials Science and Engineering A, 226–228 (1999), 151–156.